Cu/αβ-Mo$_x$C as a Highly Selective Catalyst for the Reverse Water-gas Shift Reaction

Z. Yao,[a,*] S. Liu,[a] Q. Rong,[a,b] D. Liu,[a] K. Wang,[c] and N. Sun[a,*]

[a]School of Petrochemical Engineering, Liaoning Petrochemical University, Fushun, 113001, P.R. China

[b]School of Chemical Engineering, University of Science and Technology Liaoning, Anshan 114051, China

[c]PetroChina Company Limited. Fushun Petrochemical Company, Fushun, 113004, China

The Mo carbide has been widely studied as a promising catalyst system for reverse water-gas shift reaction (RWGS). In this study, a novel Cu-doped Mo carbide, denoted as Cu/αβ-Mo$_x$C, was synthesized through a resin-based carbothermal reduction method, and its structure was characterized using XRD, BET, SEM and TEM techniques. The catalyst's Mo carbide component consisted of α-MoC$_{1-x}$ and β-Mo$_2$C phases, and the Cu/Mo molar ratios of 1/36, 1/22, 1/13, and 1/9 were considered. Among these catalysts, Cu/αβ-Mo$_x$C with a 1:22 Cu:Mo molar ratio exhibited the highest RWGS performance. It is worth noting that this catalyst also demonstrated significantly higher CO selectivity compared to previously reported Cu/β-Mo$_2$C (97.6 % vs. 89.4 %) at lower temperatures (e.g., 250 °C), attributable to its reduced affinity with CO.
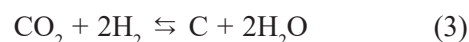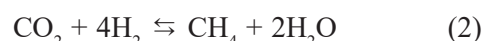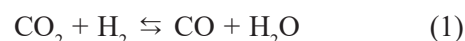
Keywords

Cu-doped Mo carbide, Cu/αβ-Mo$_x$C, resin, carbothermal reduction, reverse water-gas shift reaction

Introduction

Global warming, primarily driven by anthropogenic emissions of CO$_2$ resulting from the combustion of fossil fuels in industrial processes, energy production, and transportation, has emerged as a serious challenge in the 21st century[1]. Consequently, there is an urgent need for the development of techniques for CO$_2$ capture and storage, or catalytic conversion. To date, only a small fraction of emitted CO$_2$ has been recycled through processes such as urea, polycarbonate synthesis, and salicylic acid production[2]. In the context of the carbon neutral concept, one pivotal aspect is the transformation of CO$_2$ waste through catalytic conversion into a useful feedstock. CO$_2$ reduction to CO using H$_2$ as a reducing agent, a reaction commonly known as the reverse water gas shift (RWGS) reaction (Eq. 1), stands out as one of the most promising CO$_2$ conversion processes for its ability to produce CO, which can further be converted into various liquid fuels and high-value oxygenates through methanol synthesis and downstream Fischer-Tropsch process[3]. Notably, there are two main competing reactions (Eqs. 2 and 3), that occur alongside the RWGS reaction. The RWGS and Bosch reactions (Eqs. 1

and 3) are endothermic, and they become more prominent at higher temperatures. In contrast, the methanation reaction (eq. 2) is exothermic, making lower temperatures preferable[4].

$$CO_2 + H_2 \leftrightarrows CO + H_2O \qquad (1)$$

$$CO_2 + 4H_2 \leftrightarrows CH_4 + 2H_2O \qquad (2)$$

$$CO_2 + 2H_2 \leftrightarrows C + 2H_2O \qquad (3)$$

However, catalysts can face deactivation due to coking and sintering under high reaction temperatures. Additionally, elevated temperatures raise equipment requirements and energy consumption, increasing the production costs, and thereby limiting the industrial application of the RWGS reaction[5]. Therefore, the development of an economical catalyst with high activity and selectivity is a prerequisite for the large-scale application of the RWGS reaction. Cu-based catalysts have been extensively studied in the context of the RWGS reaction owing to their excellent catalytic activity and low price. Some investigations have shown that the catalytic performance of copper-based catalysts was mainly determined by metal size[6], promoters[7], support type and size[7–9]. Pohar and co-workers synthesized copper-based catalysts with various supports (Al$_2$O$_3$, CeO$_2$, SiO$_2$, TiO$_2$, and ZrO$_2$) and found that the choice of support affected the catalytic pathway

*Corresponding author: Zhiwei Yao (e-mail: mezhiwei@163.com) and Na Sun (e-mail: sunna@lnpu.edu.cn)

mechanisms[7]. Likozar and co-workers reported that the size of the active copper area on top of the SrTiO$_3$ perovskite catalyst support can affect activity, selectivity, and stability[9].

After molybdenum carbide catalysts were discovered to exhibit unique catalytic performance similar to noble metals in CO$_2$ reforming of CH$_4$ and water-gas shift reaction[10–13], they have been employed as new catalysts for the RWGS reaction[14–26]. It was observed that monometallic Mo$_2$C and bimetallic Co-Mo$_2$C were more active and selective for CO$_2$ conversion to CO than precious metal based bimetallic catalysts (PtCo/CeO$_2$ and PdNi/CeO$_2$)[23]. In general, Cu-based oxide catalysts have been extensively studied in the context of the RWGS reaction owing to their excellent catalytic activity and selectivity[27–29]. However, traditional Cu catalysts, such as Cu/SiO$_2$, tend to deactivate dramatically under working conditions due to the segregation of supported Cu particles at temperatures exceeding 280 °C [30]. Notably, a Cu/β-Mo$_2$C catalyst exhibited excellent catalytic activity, with mass specific rate about 5 times higher than that of the commercial Cu/ZnO/Al$_2$O$_3$ catalyst[16,24]. Moreover, Cu/β-Mo$_2$C demonstrated stability not only under steady-state conditions but also under start-up cool-down conditions. This was attributed to the strong interaction between Cu and β-Mo$_2$C, which effectively promoted the dispersion of supported Cu and prevented the aggregation of Cu particles even at temperatures as high as 600 °C[16]. These results proved the superior stabilizing properties of β-Mo$_2$C as a support material compared to traditional supports. In this study, a type of Cu/αβ-Mo$_x$C catalyst was synthesized using a straightforward resin-based carbothermal reduction method. It was observed that the Cu/αβ-Mo$_x$C catalyst exhibited higher CO selectivity than Cu/β-Mo$_2$C when subjected to similar CO$_2$ conversion conditions in the RWGS reaction.

Experimental

Materials

The raw resin used was a D201×1 cinnamic strong alkali anion exchange resin (purchased from HangZhou YongZhou Water Treatment Technology Co., Ltd.). (NH$_4$)$_6$Mo$_7$O$_{24}$·4H$_2$O (AR) and Cu(NO$_3$)$_2$·3H$_2$O (AR) were purchased from Sinopharm Chemical Reagent Co., Ltd.

Sample preparation

Firstly, the raw resin was washed with deionized water and dried at 110 °C for 12 h. Subsequently, it was ground into a fine powder. The resin powder (2.0 g) was stirred in (NH$_4$)$_6$Mo$_7$O$_{24}$·4H$_2$O

solution with a Mo atom concentration of 0.5 mol L^{-1} for 5 h. Following this, the exchanged resin was washed with deionized water three times and dried at 110 °C for 12 h. The Mo content in the dry resin was determined by ICP-AES to be 28.4 wt%. The dry resin was then impregnated with Cu(NO$_3$)$_2$·3H$_2$O solution with a given Cu/Mo molar ratio of R (R=1/36, 1/22, 1/13, and 1/9), and subsequently dried overnight at 110 °C. The resulting precursors were heated from room temperature (RT) to 900 °C at a rate of 10 °C min^{-1} under Ar (50 mL min^{-1}) and held at this temperature for 1 h. They were then cooled to RT under Ar, and then passivated in a 1 %O$_2$/Ar flow for 2 h.

Sample characterizations

X-ray diffraction (XRD) measurements were conducted using an X-ray diffractometer (X'Pert Pro MPD) equipped with a Cu Kα source. BET surface area data were obtained from a surface area analyzer (NOVA4200). The morphologies of the samples were characterized using scanning electron microscopy (SEM, Hitachi S-4800) equipped with energy dispersive X-ray spectroscopy (EDX) and transmission electron microscopy (TEM, Philips Tecnal 10). The Mo content in the dry resin was determined by inductively coupled plasma-atomic emission spectroscopy (ICP-AES). CO-temperature programmed desorption (CO-TPD) experiments were conducted in a quartz tube micro-reactor. Before the CO-TPD process, 0.1 g of catalyst was heated from RT to 900 °C in Ar and held at this temperature for 30 min. After cooling to RT, a stream of 1 %CO/He was introduced into the system for 30 min. Subsequent to CO adsorption, the gas flow was switched to He (30 mL min^{-1}) to remove physically adsorbed CO on the catalyst surface. Finally, the sample was heated from RT to 900 °C at a rate of 10 °C min^{-1} in He (30 mL min^{-1}). The effluent gases were monitored using a GC thermal conductivity detector.

Catalyst performance tests

The catalytic activities of the catalysts for RWGS were evaluated in a micro-reactor with an inner diameter of 8 mm at atmospheric pressure. Prior to the reaction, the sample was preheated in Ar at 900 °C for 0.5 h. Following the pretreatment, a gas mixture (H$_2$:CO$_2$=2:1) was passed through the catalyst with a WHSV of 60000 cm^3 g^{-1} h^{-1}. The reaction temperature range and time were 250–600 °C and 1 h, respectively. The exit gas stream from the reactor passed through a cold trap to remove water. The flow rates were measured with a soap bubble flow meter. The gas-phase products were analyzed on-line by gas chromatography (GC) equipped with

a thermal conductivity detector and a TDX-01 (60–80 mesh) packed column (300 mm×2 mm i.d.). Quantitative analysis was performed using the external standard method. A linear relationship was established between the peak area values and the volume concentration of gases in the range of 0.1–100 vol.%. The molar fractions for the products and reactants were determined based on the peak area-volume concentration curve and were taken into account in the calculation of the conversion and product distribution. The conversion of CO_2 and the selectivities of CO and CH_4 were defined as follows[16]:

$$CO_2 \text{ conversion (\%)} = ([CO_2]_{in} - [CO_2]_{out})/([CO_2]_{in}) \cdot 100$$

$$CO \text{ selectivity (\%)} = ([CO]_{out})/([CO]_{out} + [CH_4]_{out}) \cdot 100$$

$$CH_4 \text{ selectivity (\%)} = ([CH_4]_{out})/([CO]_{out} + [CH_4]_{out}) \cdot 100$$

Results and discussion

Fig. 1 shows the XRD pattern of fresh Cu- and Mo-containing carbide catalysts prepared using the resin-based carbothermal reduction method. The main peaks at 2θ of 34.5, 38.1, 39.4 and 61.6° can be attributed to the (100), (002), (101) and (110) reflections of β-Mo_2C (JCPDS 35-0787). Additionally, the characteristic diffraction peaks associated with α-MoC_{1-x} (JCPDS 65-0280) were observed at 2θ of 36.6 and 42.4°, corresponding to (111) and (200) reflections, respectively. In addition to the patterns of Mo carbide, diffractions of metallic Cu crystallites appeared at 43.3, 50.4 and 74.1°, corresponding to (111), (200) and (220) reflections, respectively. It was evident that the peak intensity associated with Cu increased with an increase in
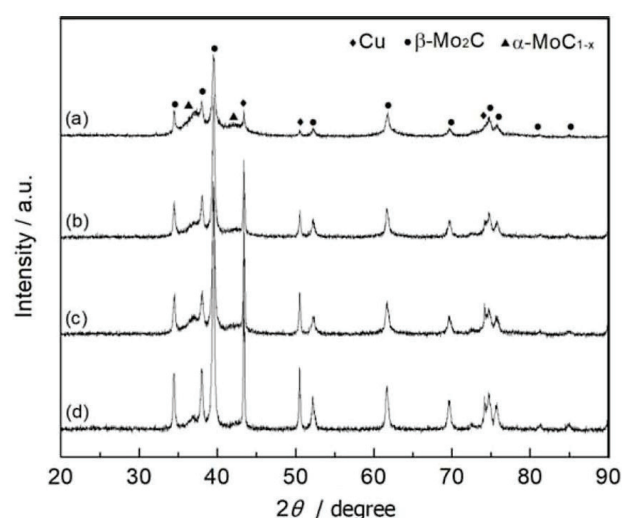

F i g. 1 – *XRD patterns of fresh Cu- and Mo-containing carbide catalysts (a) Cu/Mo=1/36, (b) Cu/Mo=1/22, (c) Cu/Mo=1/13, and (d) Cu/Mo=1/9*

T a b l e 1 – *Textural properties of the Cu/αβ-MoₓC catalysts obtained in this study*

Sample	S_{BET} (m² g⁻¹)	D_p (nm)	V_p (cm³ g⁻¹)
Carbonized resin	2.3	14.80	0.009
Cu/αβ-MoₓC (1/36)	218.4	6.58	0.29
Cu/αβ-MoₓC (1/22)	207.2	5.60	0.27
Cu/αβ-MoₓC (1/13)	198.9	4.35	0.24
Cu/αβ-MoₓC (1/9)	190.6	4.17	0.20

S_{BET} = BET surface area; D_p = Average pore diameter; V_p = Total pore volume.

T a b l e 2 – *SEM/EDX surface elemental analysis results*

Sample	Cu (wt%)	Mo (wt%)	C (wt%)	O (wt%)	Cu/Mo atomic ratio
Cu/αβ-MoₓC (1/36)	1.25	70.22	20.52	8.01	1/37.2
Cu/αβ-MoₓC (1/22)	2.16	69.56	19.58	8.71	1/21.3
Cu/αβ-MoₓC (1/13)	3.15	62.78	25.12	8.95	1/13.2
Cu/αβ-MoₓC (1/9)	4.95	65.13	21.31	8.61	1/8.7

Cu/Mo molar ratio ranging from 1/36 to 1/9. Based on the Cu/Mo molar ratio, these fresh catalysts were designated as Cu/αβ-MoₓC (1/36), Cu/αβ-MoₓC (1/22), Cu/αβ-MoₓC (1/13), and Cu/αβ-MoₓC (1/9), respectively. Subsequently, the textural properties of these Cu/αβ-MoₓC catalysts were obtained and are listed in Table 1. It was evident that the S_{BET}, D_p, and V_p of the catalysts decreased monotonically with an increase in Cu/Mo molar ratio. The obtained high surface areas of Cu/αβ-MoₓC were attributed to the intimate contact between particles and carbon species formed during the resin carbonization process[31].

The morphologies of these Cu/αβ-MoₓC catalysts were investigated using SEM and TEM (Figs. 2 and 3). It was apparent that these Cu/αβ-MoₓC catalysts exhibited similar SEM or TEM images regardless of Cu/Mo molar ratio. Irregularly shaped particles were observed on the supports, which should be assigned to carbon, as previously suggested[31–33]. The insets in Fig. 3 clearly depict the crystal lattices of Cu (111), α-MoC_{1-x} (111) and β-Mo_2C (002), confirming the presence of Cu, α-MoC_{1-x} and β-Mo_2C in these samples. These results are consistent with the observations in the XRD patterns (Fig. 1). Furthermore, EDX results (Table 2) indicated the presence of Cu, Mo, C and O elements in Cu/αβ-MoₓC (1/36), Cu/αβ-MoₓC (1/22), Cu/αβ-MoₓC (1/13), and Cu/αβ-MoₓC (1/9), and their Cu/Mo atomic ratios were close to the expected ratios of 1/36, 1/22, 1/13 and 1/9, respectively. The size dis-
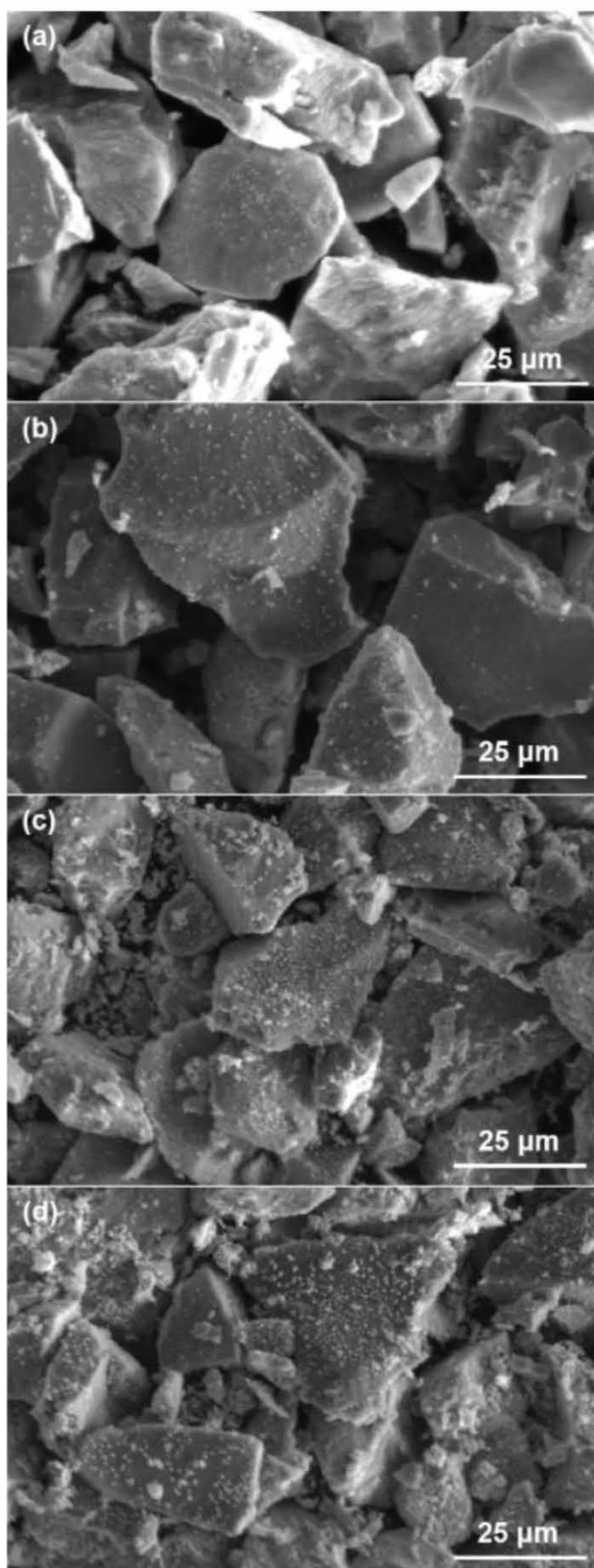
Fig. 2 – *SEM images of (a) Cu/αβ-Mo$_x$C (1/36), (b) Cu/αβ-Mo$_x$C (1/22), (c) Cu/αβ-Mo$_x$C (1/13), and (d) Cu/αβ-Mo$_x$C (1/9)*
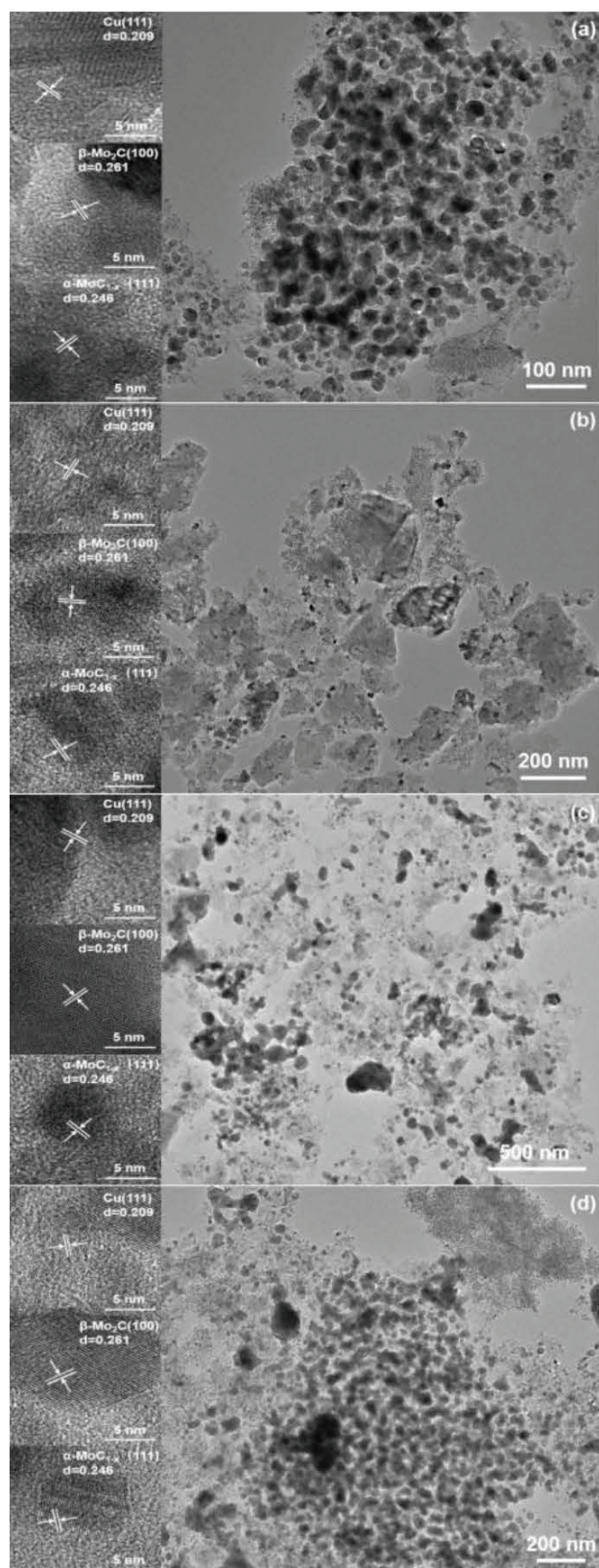
Fig. 3 – *TEM images of (a) Cu/αβ-Mo$_x$C (1/36), (b) Cu/αβ-Mo$_x$C (1/22), (c) Cu/αβ-Mo$_x$C (1/13), and (d) Cu/αβ-Mo$_x$C (1/9). The insets show the crystal lattices of Cu (111), α-MoC$_{1-x}$ (111), and β-Mo$_2$C (002).*

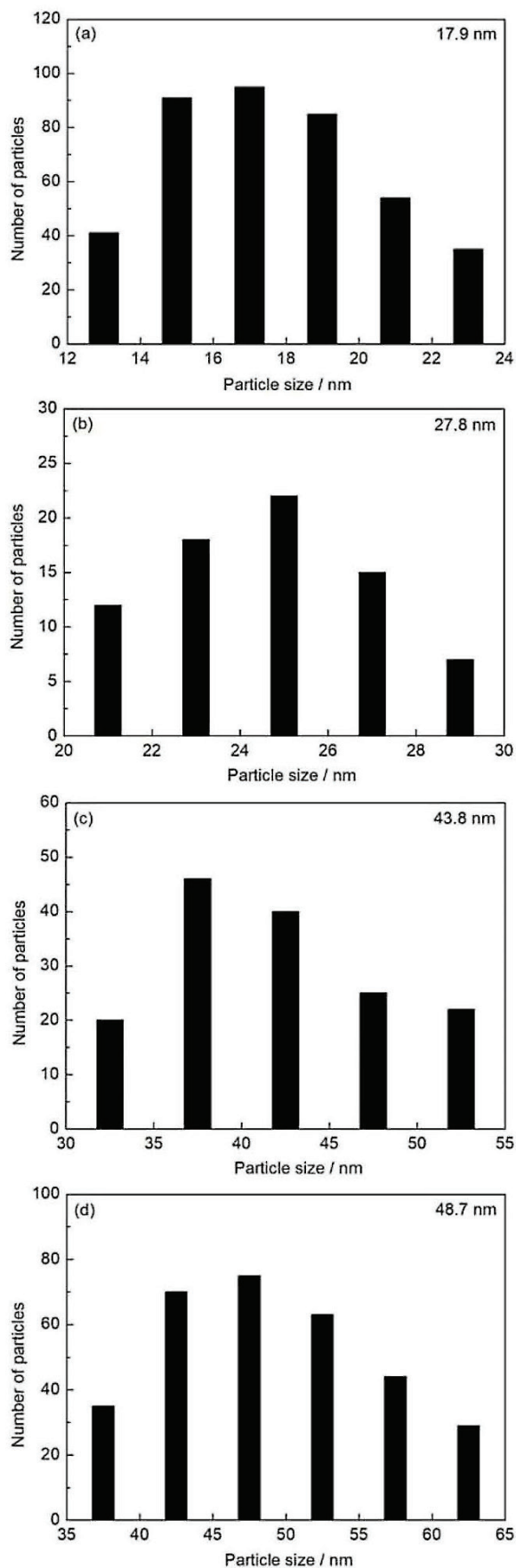Fig. 4 – *Particle size distributions in (a) Cu/αβ-Mo$_x$C (1/36), (b) Cu/αβ-Mo$_x$C (1/22), (c) Cu/αβ-Mo$_x$C (1/13), and (d) Cu/αβ-Mo$_x$C (1/9) samples*
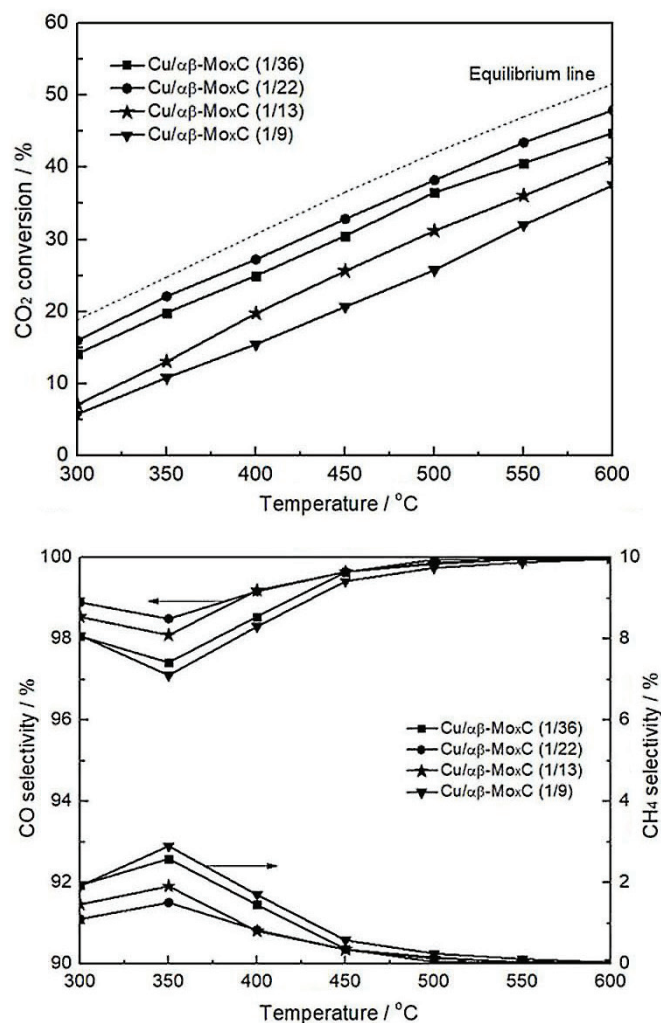
Fig. 5 – *Catalytic performance of Cu/αβ-Mo$_x$C catalysts in the RWGS reaction (CO$_2$/H$_2$ =1/2, WHSV=60000 cm^3 g^{-1} h^{-1}, P= 1 atm, T=300–600 ^{o}C)*

tributions of these nanoparticles in the Cu/αβ-Mo$_x$C (1/36), Cu/αβ-Mo$_x$C (1/22), Cu/αβ-Mo$_x$C (1/13), and Cu/αβ-Mo$_x$C (1/9) samples were determined by measuring particle size directly from TEM images (Fig. 3). It can be observed from Fig. 4 that the average particle size varied with Cu/Mo molar ratio. Specifically, it was 17.9 nm in Cu/αβ-Mo$_x$C (1/36), 27.8 nm in Cu/αβ-Mo$_x$C (1/22), 43.8 nm in Cu/αβ-Mo$_x$C (1/13), and 48.7 nm in Cu/αβ-Mo$_x$C (1/9), respectively.

The influence of Cu/Mo molar ratio on RWGS activity and selectivity is displayed in Fig. 5. Clearly, the activity followed the order of Cu/αβ-Mo$_x$C (1/22) > Cu/αβ-Mo$_x$C (1/36) > Cu/αβ-Mo$_x$C (1/13) > Cu/αβ-Mo$_x$C (1/9) across the entire temperature range. On the selectivity side, Cu/αβ-Mo$_x$C (1/22) also exhibited the highest CO selectivity and the lowest CH$_4$ selectivity. This can be attributed to the catalyst's combination of an appropriate Cu content with larger surface area and smaller particle size (Table 1 and Fig. 4). Notably, the CO selectivity first
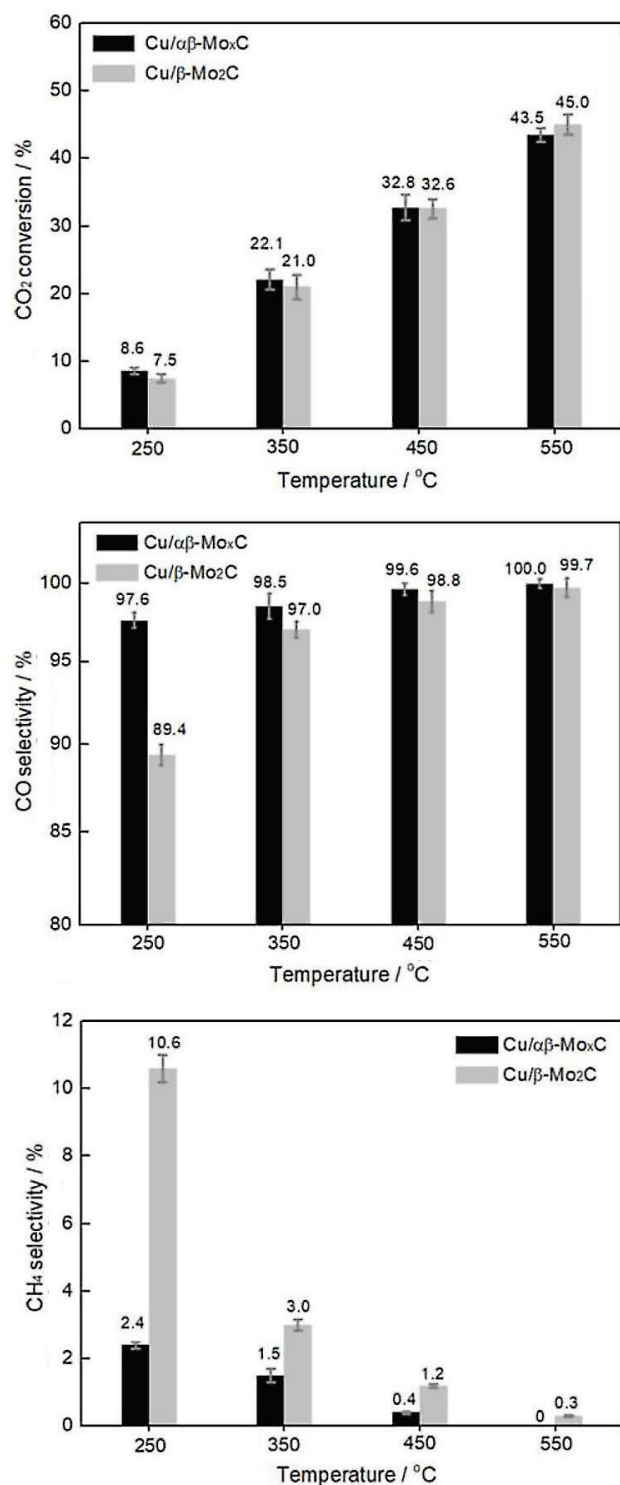
F i g . 7 – *CO-TPD curves of Cu/αβ-Mo$_x$C and Cu/β-Mo$_2$C catalysts*

F i g . 6 – *Catalytic performance of Cu/αβ-Mo$_x$C and Cu/β-Mo$_2$C catalysts in the RWGS reaction (CO$_2$/H$_2$ =1/2, WHSV=60000 cm^3 g^{-1} h^{-1}, P= 1 atm, T=250–550 °C)*

decreased and then increased in the temperature range of 300–600 °C. This was due to the enhancement of the side reaction (methanation) with a temperature rise from 300 to 350 °C. However, in the higher temperature range (>350 °C), the thermodynamic factors drove the decline in methanation activity, and CO desorption became faster, preventing
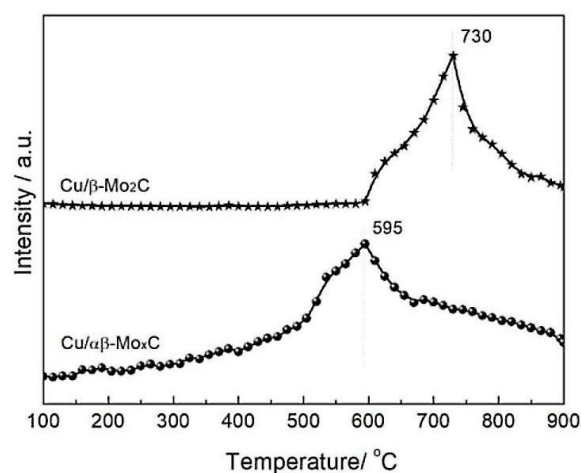
further hydrogenation to CH$_4$ on the catalyst surface[20]. Additionally, Cu/αβ-Mo$_x$C (1/22) also demonstrated excellent catalytic stability. Under conditions of WHSV=60000 cm^3 g^{-1} h^{-1} at 400 °C (not shown), it maintained ~27 % CO$_2$ conversion and ~99.5 % CO selectivity throughout the test period of 30 h. Cu/αβ-Mo$_x$C (1/22) exhibited the carbon balance value of about 99 % throughout, indicating minimal carbon deposition on the catalyst. Interestingly, there was no obvious increase in CO$_2$ conversion with the load at the starting period, likely due to the catalyst's induction period having concluded within the first hour. A similar phenomenon was observed on Mo carbide clusters in a previous study[14].

Finally, the catalytic performance of Cu/αβ-Mo$_x$C (1/22) obtained through the resin-based carbothermal reduction method in this work was compared with that of Cu/β-Mo$_2$C (with an optimized Cu loading of 1 wt%[16,24]) under similar conditions (Fig. 6). It is evident that they exhibited similar CO$_2$ conversion in the temperature range of 250–550 °C, but Cu/αβ-Mo$_x$C displayed higher CO selectivity (lower CH$_4$ selectivity) compared to Cu/β-Mo$_2$C. Furthermore, the RWGS performance of Cu/αβ-Mo$_x$C (1/22) was compared with other catalysts reported in the literature. As shown in Table 3, the Cu/αβ-Mo$_x$C catalyst exhibited superior activity and selectivity compared to traditional Pt- and Cu-based catalysts.

Generally, RWGS selectivity is directly associated with the CO adsorption properties of the catalyst[37]. The CO adsorption properties of Cu/αβ-Mo$_x$C and Cu/β-Mo$_2$C catalysts were estimated through CO-TPD, as presented in Fig. 7. It is evident that both catalysts exhibited desorption peaks in the CO-TPD curves. Clearly, the desorption peak temperature corresponding to Cu/αβ-Mo$_x$C (595 °C) was lower than that of Cu/β-Mo$_2$C (730 °C), indicating

Table 3 – *Comparison of CO$_2$ conversion and CO selectivity for Cu/αβ-Mo$_x$C and the literature reported catalysts*

Catalyst	H$_2$:CO ratio	Temperature (°C)	WHSV (cm^3 g^{-1} h^{-1})	CO$_2$ conversion (%)	CO selectivity (%)	Ref.
Cu/αβ-Mo$_x$C	2:1	300	60000	16.0	98.9	this work
	2:1	400	60000	27.2	99.2	this work
	2:1	500	60000	38.2	99.8	this work
	2:1	600	60000	47.9	100	this work
Cu-Zn-Al	2:1	500	300000	21.0	100	16
Pt-Al$_2$O$_3$	1.4:1	400	12000	6.4	N/A	34
Pt-TiO$_2$	1.4:1	400	12000	16.0	N/A	34
Cu-Al$_2$O$_3$	1:9	500	12000	20.1	100	35
Ni-CeO$_2$	1:1	400	120000	9.0	77	36

that Cu/β-Mo$_2$C exhibited a stronger affinity with CO. In other words, during the RWGS reaction, the CO product adsorbed on Cu/β-Mo$_2$C could dissociate more easily and be further hydrogenated to CH$_4$. This likely explains why Cu/β-Mo$_2$C exhibited lower CO selectivity compared to Cu/αβ-Mo$_x$C.

Conclusions

A series of Cu-doped Mo carbide catalysts with varying Cu/Mo molar ratios (1/36, 1/22, 1/13, and 1/9) were synthesized using resin-based carbothermal reduction method. The resulting materials were characterized through XRD, BET, SEM, TEM and CO-TPD techniques. The S_{BET}, D_P, and V_p of the catalysts decreased monotonically with the increase in Cu/Mo molar ratio. The obtained high surface areas of Cu/αβ-Mo$_x$C were attributed to the intimate contact between particles and carbon species. The catalytic activities of these Cu/αβ-Mo$_x$C catalysts were assessed using RWGS as the reaction probe. Among these catalysts, Cu/αβ-Mo$_x$C (1/22) exhibited the best RWGS activity and selectivity, likely due to the fact that the catalyst combined an appropriate Cu content with larger surface area and smaller particle size. It is worth noting that Cu/αβ-Mo$_x$C (1/22) also demonstrated significantly higher CO selectivity than the previously reported Cu/β-Mo$_2$C (97.6 % vs. 89.4 %) at lower temperatures (e.g., 250 °C), primarily owing to its weaker affinity with CO.

References

1. *González-Castaño, M., Dorneanu, B., Arellano-García, H.,* The reverse water gas shift reaction: A process systems engineering perspective, React. Chem. Eng. **6** (2021) 954.
doi: https://doi.org/10.1039/D0RE00478B

2. *Hansen, J., Sato, M., Ruedy, R., Lo, K., Lea, D. W., Medina-Elizade, M.,* Global temperature change, Proc. Natl. Acad. Sci. U.S.A. **103** (2006) 14288.
doi: https://doi.org/10.1073/pnas.0606291103

3. *Marchese, M., Buffo, G., Santarelli, M., Lanzini, A.,* CO$_2$ from direct air capture as carbon feedstock for Fischer-Tropsch chemicals and fuels: Energy and economic analysis, J. CO$_2$ Util. **46** (2021) 101487.
doi: https://doi.org/10.1016/j.jcou.2021.101487

4. *Le Saché, E., Pastor-Pérez, L., Haycock, B. J., Villora-Picó, J. J., Sepúlveda-Escribano, A., Reina, T. R.,* Switchable catalysts for chemical CO$_2$ recycling: A step forward in the methanation and reverse water-gas shift reactions, ACS Sustainable Chem. Eng. **8** (2020) 4614.
doi: https://doi.org/10.1021/acssuschemeng.0c00551

5. *Zhou, G., Dai, B., Xie, H., Zhang, G., Xiong, K., Zheng, X.,* CeCu composite catalyst for CO synthesis by reverse water–gas shift reaction: Effect of Ce/Cu mole ratio, J. CO$_2$ Util. **21** (2017) 292.
doi: https://doi.org/10.1016/j.jcou.2017.07.004

6. *Wu, H. C., Chang, Y. C., Wu, J. H., Lin, J. H., Lin, I. K., Chen, C. S.,* Methanation of CO$_2$ and reverse water gas shift reactions on Ni/SiO$_2$ catalysts: The influence of particle size on selectivity and reaction pathway, Catal. Sci. Technol. **5** (2015) 4154.
doi: https://doi.org/10.1039/c5cy00667h

7. *Jurković, D. L., Pohar, A., Dasireddy, V. D. B. C., Likozar, B.,* Effect of copper-based catalyst support on reverse water-gas shift reaction (RWGS) activity for CO$_2$ reduction, Chem. Eng. Technol. **40** (2017) 973.
doi: https://doi.org/10.1002/ceat.201600594

8. *Jurković, D. L., Prašnikar, A., Pohar, A., Likozar, B.,* Surface structure-based CO$_2$ reduction reaction modelling over supported copper catalysts, J. CO$_2$ Util. **41** (2020) 101234.
doi: https://doi.org/10.1016/j.jcou.2020.101234

9. *Kopač, D., Likozar, B., Huš, M.,* How size matters: Electronic, cooperative and geometric effect in perovskite-supported copper catalysts for CO$_2$ reduction, ACS Catal. **10** (2020) 4092.
doi: https://doi.org/10.1021/acscatal.9b05303

10. *Patt, J., Moon, D. J., Phillips, C., Thompson, L.,* Molybdenum carbide catalysts for water-gas shift, Catal. Lett. **65** (2000) 193.
doi: https://doi.org/10.1023/a:1019098112056

11. *Zhang, L., Yang, Y., Yao, Z., Yan, S., Kang, X.,* Finding of a new cycle route in Ni/Mo$_2$C catalyzed CH$_4$-CO$_2$ reforming, Catal. Sci. Technol. **11** (2021) 479.
doi: https://doi.org/10.1039/D0CY02428G

12. *Gao, H., Yao, Z., Shi, Y., Jia, R., Liang, F., Sun, Y., Mao, W., Wang, H.,* Simple and large-scale synthesis of β-phase molybdenum carbides as highly stable catalysts for dry reforming of methane, Inorg. Chem. Front. **5** (2018) 90.
doi: https://doi.org/10.1039/C7QI00532F

13. *Gao, H., Yao, Z., Shi, Y., Wang, S.,* Improvement of the catalytic stability of molybdenum carbide via encapsulation within carbon nanotubes in dry methane reforming, Catal. Sci. Technol. **8** (2018) 697.
doi: https://doi.org/10.1039/C7CY02506H

14. *Ma, Y., Guo, Z., Jiang, Q., Wu, K.-H., Gong, H., Liu, Y.,* Molybdenum carbide clusters for thermal conversion of CO$_2$ to CO via reverse water-gas shift reaction, J. Energy Chem. **50** (2020) 37.
doi: https://doi.org/10.1016/j.jechem.2020.03.012

15. *Reddy, K. P., Dama, S., Mhamane, N. B., Ghosalya, M. K., Raja, T., Satyanarayana, C. V., Gopinath, C. S.,* Molybdenum carbide catalyst for the reduction of CO$_2$ to CO: Surface science aspects by NAPPES and catalysis studies, Dalton Trans. **48** (2019) 12199.
doi: https://doi.org/10.1039/C9DT01774G

16. *Zhang, X., Zhu, X., Lin, L., Yao, S., Zhang, M., Liu, X., Wang, X., Li, Y.-W., Shi, C., Ma, D.,* Highly dispersed copper over β-Mo$_2$C as an efficient and stable catalyst for the reverse water gas shift (RWGS) reaction, ACS Catal. **7** (2017) 912.
doi: https://doi.org/10.1021/acscatal.6b02991

17. *Heracleous, E., Koidi, V., Lappas, A. A.,* CO$_2$ conversion over Cu-Mo$_2$C catalysts: Effect of the Cu promoter and preparation method, Catal. Sci. Technol. **11** (2021) 1467.
doi: https://doi.org/10.1039/D0CY02021D

18. *Dasireddy, V. D. B. C., Vengust, D., Likozar, B., Kovač, J., Mrzel, A.,* Production of syngas by CO$_2$ reduction through Reverse Water-Gas Shift (RWGS) over catalytically-active molybdenum-based carbide, nitride and composite nanowires, Renewable Energy **176** (2021) 251.
doi: https://doi.org/10.1016/j.renene.2021.05.051

19. *Marquart, W., Raseale, S., Prieto, G., Zimina, A., Sarma, B. B., Grunwaldt, J.-D., Claeys, M., Fischer, N.,* CO$_2$ reduction over Mo$_2$C-based catalysts, ACS Catal. **11** (2021) 1624.
doi: https://doi.org/10.1021/acscatal.0c05019

20. *Gao, J., Wu, Y., Jia, C., Zhong, Z., Gao, F., Yang, Y., Liu, B.,* Controllable synthesis of α-MoC$_{1-x}$ and β-Mo$_2$C nanowires for highly selective CO$_2$ reduction to CO, Catal. Commun. **84** (2016) 147.
doi: https://doi.org/10.1016/j.catcom.2016.06.026

21. *Porosoff, M. D., Baldwin, J. W., Peng, X., Mpourmpakis, G., Willauer, H. D.,* Potassium-promoted molybdenum carbide as a highly active and selective catalyst for CO$_2$ conversion to CO, ChemSusChem. **10** (2017) 2408.
doi: https://doi.org/10.1002/cssc.201700412

22. *Posada-Pérez, S., Viñes, F., Ramirez, P. J., Vidal, A. B., Rodriguez, J. A., Illas, F.,* The bending machine: CO$_2$ activation and hydrogenation on δ-MoC(001) and β-Mo$_2$C(001) surfaces, Phys. Chem. Chem. Phys. **16** (2014) 14912.
doi: https://doi.org/10.1039/C4CP01943A

23. *Porosoff, M. D., Yang, X., Boscoboinik, J. A., Chen, J. G.,* Molybdenum carbide as alternative catalysts to precious metals for highly selective reduction of CO$_2$ to CO, Angew. Chem. Int. Ed. **53** (2014) 6705.
doi: https://doi.org/10.1002/anie.201404109

24. *Zhang, Q., Pastor-Pérez, L., Jin, W., Gu, S., Reina, T. R.,* Understanding the promoter effect of Cu and Cs over highly effective β-Mo$_2$C catalysts for the reverse water-gas shift reaction, Appl. Catal., B. **244** (2019) 889.
doi: https://doi.org/10.1016/j.apcatb.2018.12.023

25. *Liu, X., Kunkel, C., Pilar Ramirez de la Piscina, P., Homs, N., Viñes, F., Illas, F.,* Effective and highly selective CO generation from CO using a polycrystalline α-MoC catalyst, ACS. Catal. **7** (2017) 4323.
doi: https://doi.org/10.1021/acscatal.7b00735

26. *Porosoff, M. D., Kattel, S., Li, W., Liu, P., Chen, J. G.,* Identifying trends and descriptors for selective CO$_2$ conversion to CO over transition metal carbides, Chem. Commun. **51** (2015) 6988.
doi: https://doi.org/10.1039/C5CC01545F

27. *Porosoff, M. D., Yan, B., Chen, J. G.,* Catalytic reduction of CO$_2$ by H$_2$ for synthesis of CO, methanol and hydrocarbons: Challenges and opportunities, Energy Environ. Sci. **9** (2016) 62.
doi: https://doi.org/10.1039/C5EE02657A

28. *Gao, P., Li, F., Zhan, H., Zhao, N., Xiao, F., Wei, W., Zhong, L., Wang, H., Sun, Y.,* Influence of Zr on the performance of Cu/Zn/Al/Zr catalysts via hydrotalcite-like precursors for CO$_2$ hydrogenation to methanol, J. Catal. **298** (2013) 51.
doi: https://doi.org/10.1016/j.jcat.2012.10.030

29. *Arena, F., Mezzatesta, G., Zafarana, G., Trunfio, G., Frusteri, F., Spadaro, L.,* Effects of oxide carriers on surface functionality and process performance of the Cu-ZnO system in the synthesis of methanol via CO$_2$ hydrogenation, J. Catal. **300** (2013) 141.
doi: https://doi.org/10.1016/j.jcat.2012.12.019

30. *Yue, H., Zhao, Y., Zhao, S., Wang, B., Ma, X., Gong, J.,* A copper-phyllosilicate core-sheath nanoreactor for carbon–oxygen hydrogenolysis reactions, Nat. Commun. **4** (2013) 2339.
doi: https://doi.org/10.1038/ncomms3339

31. *Yao, Z., Tong, J., Qiao, X., Jiang, J., Zhao, Y., Liu, D., Zhang, Y., Wang, H.,* Novel synthesis of dispersed molybdenum and nickel phosphides from thermal carbonization of metal- and phosphorus-containing resins, Dalton. Trans. **44** (2015) 19383.
doi: https://doi.org/10.1039/C5DT02464A

32. *Yan, Z., Wang, H., Zhang, M., Jiang, Z., Jiang, T., Xie, J.,* Pt supported on Mo$_2$C particles with synergistic effect and strong interaction force for methanol electro-oxidation, Electrochim. Acta. **95** (2013) 218.
doi: https://doi.org/10.1016/j.electacta.2013.02.031

33. *Liang, P., Gao, H., Yao, Z., Jia, R., Shi, Y., Sun, Y., Fan, Q., Wang, H.,* Simple synthesis of ultrasmall β-Mo$_2$C and α-MoC$_{1-x}$ nanoparticles and new insights into their catalytic mechanisms for dry reforming of methane, Catal. Sci. Technol. **7** (2017) 3312.
doi: https://doi.org/10.1039/C7CY00708F

34. *Kim, S. S., Lee, H. H., Hong, S. C.,* A study on the effect of support's reducibility on the reverse water-gas shift reaction over Pt catalysts, Appl. Catal. A. **423** (2012) 100.
doi: https://doi.org/10.1016/j.apcata.2012.02.021

35. *Chen, C., Cheng, W., Lin, S.,* Mechanism of CO formation in reverse water–gas shift reaction over Cu/Al$_2$O$_3$ catalyst, Catal. Lett. **68** (2000) 45.
doi: https://doi.org/10.1023/a:1019071117449

36. *Wang, L., Zhang, S., Liu, Y.,* Reverse water gas shift reaction over Co-precipitated Ni-CeO$_2$ catalysts, J. Rare Earths. **26** (2008) 66.
doi: https://doi.org/10.1016/s1002-0721(08)60039-3

37. *Zhao, Z., Wang, M., Ma, P., Zheng, Y., Chen, J., Li, H., Zhang, X., Zheng, K., Kuang, Q., Xie, Z.-X.,* Atomically dispersed Pt/CeO$_2$ catalyst with superior CO selectivity in reverse water gas shift reaction, Appl. Catal. B-Environ. **291** (2021) 120101.
doi: https://doi.org/10.1016/j.apcatb.2021.120101